Nanotechnology **18** (2007) 365304 (5pp) doi:10.1088/0957-4484/18/36/365304

Solid Au nanoparticles as a catalyst for growing aligned ZnO nanowires: a new understanding of the vapour–liquid–solid process

Melanie Kirkham, Xudong Wang, Zhong Lin Wang[1] and Robert L Snyder[1]

School of Materials Science and Engineering, Georgia Institute of Technology, Atlanta, GA 30332-0245, USA

E-mail: zlwang@gatech.edu and bob.snyder@mse.gatech.edu

Received 25 June 2007
Published 14 August 2007
Online at stacks.iop.org/Nano/18/365304

Abstract

X-ray diffraction techniques have been applied to characterize the Au-catalysed growth of aligned ZnO nanowire arrays on an $AlGaN/AlN/Al_2O_3$ substrate. The orientation relationships between the AlN layer, AlGaN layer, ZnO nanowires and Au particles were determined using x-ray texture analysis. Two orientations of the Au nanoparticles, related by a 30° rotation about the sample normal, were observed. The gold lattice parameter of the ZnO nanowire sample was determined to be the same as that of a control sample never exposed to vaporized ZnO, indicating the absence of Zn in the Au catalyst particles. Our results indicate that the Au catalyst particles were solid during growth, and that growth proceeded by a surface diffusion process, rather than a bulk diffusion process.

1. Introduction

Quasi-one-dimensional nanostructures of ZnO have large aspect ratios and occur in a variety of forms, including nanowires with circular cross-sections, and nanobelts with rectangular cross-sections [1]. ZnO nanostructures have many potentially useful applications, such as field emitters [1], photodetectors [2], gas sensors [3] and nanogenerators [4, 5]. However, manipulation of nanostructures into desirable configurations is a significant problem. Individual nanostructures can be moved using the probe of an atomic force microscope (AFM) [6], but the procedure cannot easily be scaled up for technological applications. A solution is to grow the nanostructures in the desired arrangement. Synthesis of arrays of aligned one-dimensional (1D) nanostructures via the vapour–liquid–solid (VLS) method has been reported in several different systems [7–10].

In the VLS synthesis mechanism, first proposed in 1964 by Wagner and Ellis for Au-catalysed Si whiskers [11], a catalyst particle, usually Au or another metal, sits on a substrate and serves as a preferential site for absorption of a vapour, often generated by thermally evaporating the desired source material. The source material absorbing into the catalyst particle causes it to melt via a eutectic reaction. Once the catalyst particle becomes supersaturated, the excess source material precipitates out and a 1D nanostructure grows.

Synthesis of nanowires has most often been attributed to the VLS mechanism. However, some studies have reported an alternate mechanism with a solid catalyst particle during growth, called the vapour–solid–solid (VSS) mechanism. In particular, solid catalyst particles have been reported for Au-catalysed III–V semiconductors [12–16], Ti- and Al-catalysed silicon [17, 18], and Au-catalysed ZnSe [19]. In most of these studies, growth was observed at temperatures below the relevant eutectic. For Au-catalysed ZnO, nanowire growth has been reported at 500 °C, almost 200 °C below the Au-rich Au–Zn eutectic temperature of 684 °C [20].

Fully understanding the mechanism of formation of these nanostructures is vital to controlling the process and may allow tailoring of their morphology and properties. The purpose of

[1] Authors to whom any correspondence should be addressed.

this study is to gain understanding of the synthesis method by characterizing an array of Au-catalysed ZnO nanowires using electron microscopy and x-ray diffraction techniques. Our results provide in-depth insight into the growth of nanowires and the role played by the Au catalyst, providing a fundamental understanding of the VLS process.

2. Experimental method

The aligned ZnO nanowires characterized in this study were synthesized through the process that we reported previously [21]. In general, a mixture of equal amounts (by weight) of ZnO and graphite powders was used as source material and was loaded in an alumina boat. The source material was located at the centre of an alumina tube. Argon was used as the carrier gas at a flow rate of 49 sccm and 2% (1 sccm) oxygen was introduced simultaneously. The substrate consisted of *c*-plane oriented, single-crystal Al_2O_3 covered with a layer of AlN followed by AlGaN, and finally coated with gold catalyst. The substrate was placed downstream in a temperature zone of ∼850 °C. A horizontal tube furnace was used to heat the source materials to 950 °C at a rate of 50 °C min^{-1} and the temperature was held at the peak temperature for 30 min under a pressure of 30 mbar for the deposition of nanowires. Then the system was cooled down to room temperature with argon flowing.

The aligned ZnO nanowires were characterized using scanning electron microscopy (SEM) and x-ray diffraction (XRD) methods, including texture analysis, discussed below. A LEO 1530 scanning electron microscope was used. XRD scans were collected with Cu Kα radiation. Parallel beam geometry was used with a Göbel mirror (equatorial divergence $< 0.05°$) in order to eliminate errors due to sample surface displacement. A 0.27° parallel plate collimator and 0.04 rad Soller slits controlled axial divergence. Six θ–2θ scans were collected for determining the ZnO lattice parameters and 14 for the Au lattice parameter of the nanowire sample. Eight rocking curves were collected on each of five reflections: Au{111}, ZnO(0002), AlGaN(0002), AlN(0002) and Al_2O_3(0006). High-temperature XRD data were collected of the Au{111} reflection of Au-catalysed ZnO nanorods in air from 500 to 1000 °C in 100 °C increments. Data were collected with a 0.4°ω offset in parafocusing geometry with Mo Kα radiation.

A control sample was prepared with 5 nm of Au thermally evaporated onto a GaN layer on *c*-plane oriented, single-crystal Al_2O_3 substrate. The sample was heated at 600 °C and then 850 °C for 30 and 60 min, respectively. The sample was analysed using SEM and XRD, including grazing incidence (GIXRD) and θ–2θ scans with an ω offset to minimize the signal from the Al_2O_3 substrate.

XRD allows information to be gathered from an entire array at once. In addition, the substrate/nanostructure interface is preserved, which is vital, since the substrate interface plays a large role in synthesis. Texture analysis, traditionally applied to deformed metals, determines the location of poles (normals) to a specified set of planes with respect to the sample orientation. The x-ray source and detector are fixed at a particular diffraction angle corresponding to the planes of interest. Intensity is recorded as the sample is rotated and tilted and is then plotted in a stereographic projection, called a pole figure. Peaks indicate crystallites oriented with the poles of the specified planes in the direction given by the rotation and tilt angles.

Texture data were collected with Cu Kα radiation, using a polycapillary x-ray lens to generate a parallel beam and placing a 0.27° parallel plate collimator and 0.04 rad Soller slits in front of the detector. The step size for both rotation and tilt was 5°, and the count time was 8 s. An $Al_2O_3\{02\bar{2}4\}$ pole figure was collected at the beginning of each session to align the sample. Overlap from intense peaks with similar *d*-spacings caused extraneous artefacts in some pole figures. This effect was minimized by choosing strong peaks with few close reflections.

Data were analysed and orientation distribution functions (ODFs) were calculated with PANalytical's Texture computer program. ODFs combine the information in several pole figures to represent the directions of the [001] poles of a particular phase in the sample with respect to the sample geometry [22]. The directions are represented using three Euler angles (ϕ_1, Φ and ϕ_2 in the Bunge notation). The angle ϕ_1 corresponds to a rotation about the normal to the sample surface, as shown in the inset in figure 1. The angle Φ corresponds to a tilt of the [001] pole away from the sample normal. The angle ϕ_2 corresponds to a rotation about the tilted [001] pole. By examining the distribution of intensity in three-dimensional ϕ_1–Φ–ϕ_2 space, the distribution of crystal orientations can be determined. ODFs were calculated from four pole figures for the AlN layer ($\{10\bar{1}0\}$, (0002), $\{10\bar{1}1\}$ and $\{10\bar{1}2\}$), three pole figures for the AlGaN layer ($\{10\bar{1}0\}$, $\{10\bar{1}2\}$ and $\{10\bar{1}3\}$), four pole figures for the ZnO nanorods ($\{10\bar{1}0\}$, $\{10\bar{1}2\}$, $\{10\bar{1}3\}$ and $\{11\bar{2}0\}$), and four pole figures for the Au particles ({111}, {200}, {220} and {311}).

3. Results and discussion

3.1. Orientation analysis

Al_2O_3, AlN, AlGaN and ZnO all have the same wurtzite crystal structure with six-fold symmetry in the basal plane. Therefore, it is expected that AlN, AlGaN and ZnO will take the same *c*-plane crystal orientation as the Al_2O_3 substrate. Since gold has the face-centred cubic (FCC) structure, the Au{111} planes have three-fold hexagonal-like symmetry, so a Au{111} orientation is also predicted.

An XRD pattern was collected on the sample, shown in figure 1. The Al_2O_3 substrate reflections have been minimized by using a 1°ω offset. For the AlN, AlGaN and ZnO, (000ℓ) reflections are present, indicating that these phases are (0001)-oriented. Au{hhh} reflections are observed, indicating that the Au is {111}-oriented.

Figure 2 displays rocking curves collected on the Al_2O_3(0006), AlN(0002), AlGaN(0002), ZnO(0002) and Au {111} reflections. The peak widths (full width at half maximum) are 0.0243° ± 0.006, 0.5107° ± 0.0006, 0.4337° ± 0.002, 0.8773° ± 0.1 and 1.7740° ± 0.01, respectively. This small degree of misalignment indicates that the nanostructures grow epitaxially and are very well aligned.

In order to further investigate the crystal orientations, texture data were collected and orientation distribution functions (figure 3) were calculated for the AlN, AlGaN, ZnO

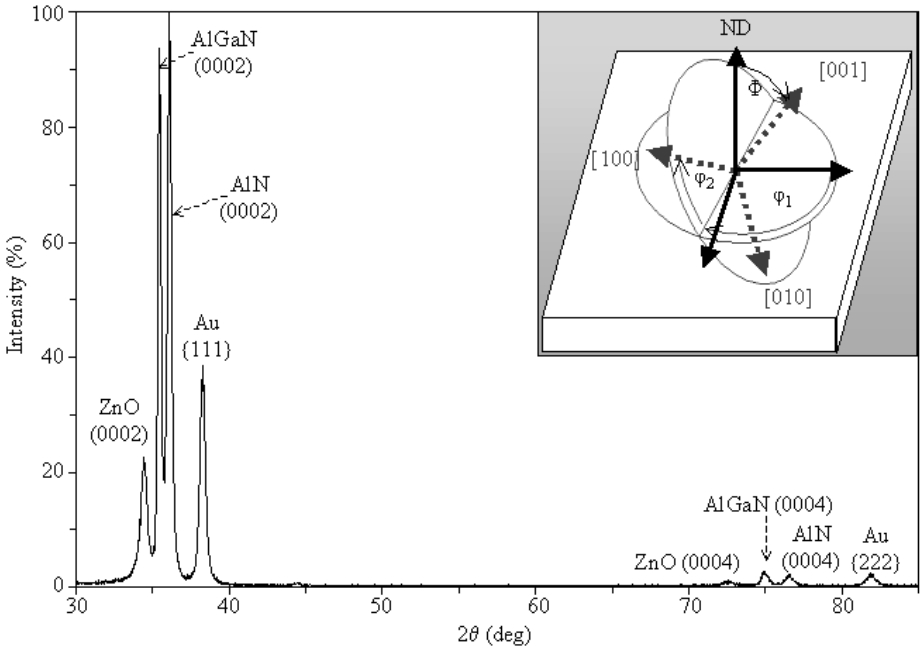

Figure 1. X-ray diffraction pattern of Au-catalysed ZnO nanorods grown on an AlN/AlGaN layer on an Al_2O_3 single-crystal (0001) substrate with 1°ω offset to reduce the substrate signal. The inset is a schematic diagram of Euler angles in the Bunge notation. ϕ_1 is a rotation about the sample normal (ND). Φ is a tilt of [001] from ND. ϕ_2 is a rotation about [001]. After Cullity and Stock [22].

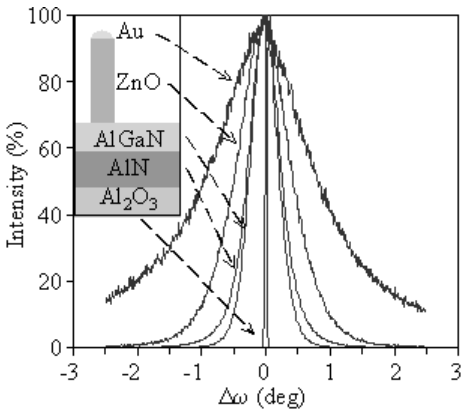

Figure 2. Rocking curves collected on the Al_2O_3(0006), AlN(0002), AlGaN(0002), ZnO(0002) and Au {111} reflections. The inset is a schematic diagram of the ZnO nanorod sample.

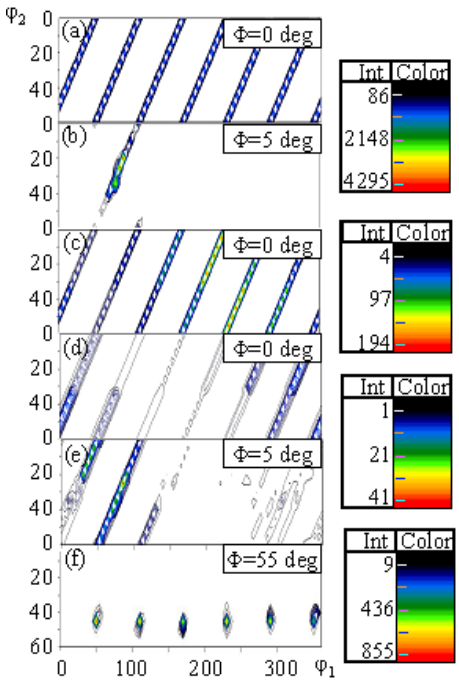

Figure 3. Orientation distribution functions of (a) and (b) AlN layer, (c) AlGaN layer, (d) and (e) ZnO nanorods, and (f) Au catalyst. Only Φ planes with significant intensity are displayed.

and Au. For AlN, only the $\Phi = 0°$ and 5° planes are shown, since no significant intensity is observed outside those planes, indicating that the AlN is (0001)-oriented, as expected. The spread of intensity into the $\Phi = 5°$ plane indicates a small degree of misalignment. For AlGaN, only the $\Phi = 0°$ plane is shown, since no significant intensity is observed outside that plane, indicating that the AlGaN is (0001)-oriented, as expected.

For ZnO, only the $\Phi = 0°$ and 5° planes are shown, since no significant intensity is observed outside those planes, indicating that the ZnO is (0001)-oriented, as expected. The spread of intensity into the $\Phi = 5°$ plane indicates a small degree of misalignment of the nanowires. For Au, only the $\Phi = 55°$ plane is shown, since no significant intensity is observed outside that plane, indicating that the Au is {111}-oriented, as seen by comparison with the calculated angle of 54.74° between the (001) and {111} poles in Au. The orientation relationships, including parallel planes and directions, are summarized in table 1.

An unexpected result from the texture analysis was the discovery of two orientations for the Au phase. In the Au ODF, six discrete points are observed at $\phi_2 = 45°$ and $\phi_1 =$

Table 1. Orientation relationships between the Au, ZnO, AlGaN, AlN and Al_2O_3 phases as determined from texture analysis.

Phase	Parallel plane	Parallel direction
Au	{111}	$\langle 11\bar{2}\rangle$
ZnO	(0001)	$\langle 01\bar{1}0\rangle$
AlGaN	(0001)	$\langle 01\bar{1}0\rangle$
AlN	(0001)	$\langle 01\bar{1}0\rangle$
Al_2O_3	(0001)	$\langle 21\bar{3}0\rangle$

$60\times n-10$, where n is an integer from 1 to 6. This indicates six in-plane rotations of 60° for the Au catalyst particles. However, the Au {111} planes have only three-fold symmetry. Therefore, the six rotations are due to two unique orientations related to each other by a 60° rotation about the sample normal, with the other rotations being generated by the trigonal symmetry of the Au {111} planes.

A closer examination of the texture data reveals some unexpected orientation relationships within the parallel interfacial planes. The parallel directions within the Al_2O_3 and AlN planes ($\langle 21\bar{3}0\rangle_{Al_2O_3} \parallel \langle 01\bar{1}0\rangle_{AlN}$) indicate a 30° rotation between the hexagonal symmetry of each plane. Though counterintuitive, this relationship actually reduces the lattice mismatch at the surface. For the observed orientation relationship, the lattice mismatch is 32% in the $\langle 21\bar{3}0\rangle_{Al_2O_3} \parallel \langle 01\bar{1}0\rangle_{AlN}$ directions and 13% in the $\langle 01\bar{1}0\rangle_{Al_2O_3} \parallel \langle 21\bar{3}0\rangle_{AlGaN}$ directions. Though somewhat large for epitaxial growth, this is still smaller than the lattice mismatch of 53% in the $\langle 01\bar{1}0\rangle_{Al_2O_3} \parallel \langle 01\bar{1}0\rangle_{AlN}$ directions. Unlike the Al_2O_3/AlGaN interface, the hexagonal symmetries of the AlN(0001) ∥ AlGaN(0001) ∥ ZnO(0001) interfaces match, with $\langle 01\bar{1}0\rangle_{AlN}$ parallel to $\langle 01\bar{1}0\rangle_{AlGaN}$ parallel to $\langle 01\bar{1}0\rangle_{ZnO}$. The lattice mismatches are small, 2%.

Similar to the Al_2O_3/AlN interface, the hexagonal symmetry of the ZnO(0001) ∥ Au{111} interface is rotated by 30°, with $\langle 01\bar{1}0\rangle_{ZnO}$ parallel to $\langle 11\bar{2}\rangle_{Au}$. The lattice mismatch is 30% in the $\langle 01\bar{1}0\rangle_{ZnO} \parallel \langle 11\bar{2}\rangle_{Au}$ directions and 2% in the $\langle 21\bar{3}0\rangle_{ZnO} \parallel \langle \bar{1}10\rangle_{Au}$ directions. These mismatches are larger in one direction and smaller in the other as compared to the mismatch of 13% if the hexagonal symmetry matched, i.e. $\langle 01\bar{1}0\rangle_{ZnO} \parallel \langle \bar{1}10\rangle_{Au}$.

3.2. Gold catalyst particle

The samples were imaged with scanning electron microscopy (SEM). The nanowires have a columnar shape, with an average length of 284 ± 72 nm, and an average diameter of 35 ± 11 nm. The catalyst particle is roughly hemispherical in shape with an average diameter, 33 ± 12 nm, similar to that of the nanowire. There is a large variation in the size of the nanostructures, as evidenced by the standard deviation values above. The nanowires are predominantly aligned vertically.

The lattice parameter of the gold in the ZnO nanorod sample was determined from XRD scans to be 4.073±0.001 Å, slightly smaller than the bulk value of 4.078 94 Å (ICSD #58393). The volume ratio of ZnO to Au is 223 ± 43 to 1, as determined from the integrated intensity of each peak. Therefore, it is unlikely that any extraneous gold is present in the sample to affect the signal from the gold catalyst particles on the ZnO nanorods. The observed decrease in Au lattice parameter, as compared to the reference value, is expected due to the known lattice contraction occurring in nanoparticles [23].

Qi and Wang [23] developed a model to quantify the change in lattice parameter, a, for metal nanoparticles as a function of the particle diameter (D) and shape, shear modulus and surface energy. For 33 nm hemispherical Au particles, the change in lattice parameter is −0.1433%, leading to an expected lattice parameter of 4.0731 Å, which is consistent with the experimentally measured Au lattice parameter of 4.073 ± 0.001 Å.

To further investigate the Au lattice parameter, a controlled sample of Au thermally evaporated on a GaN layer on c-plane oriented, single-crystal Al_2O_3 substrate was prepared and investigated with SEM and XRD. After deposition of a 5 nm layer of Au, a small number of Au nanoparticles were observed on the sample surface, and XRD patterns show evidence of polycrystalline Au, though the weak Au signal prevents detailed analysis. After annealing at 600 °C and 850 °C for 30 and 60 min, respectively, the sample is densely covered with Au nanoparticles with an average diameter of 32 ± 12 nm. An XRD pattern (with a 2°ω offset to reduce the Al_2O_3 substrate signal) indicates that the Au is primarily {111}-oriented. The Au lattice parameter of the control sample, as determined from the GIXRD and 2θ offset scans, is 4.073 ± 0.002 Å, which is the same as that measured from the ZnO nanorod sample.

The finding that the gold lattice parameters measured from both the nanowire sample and the control sample, which was not exposed to ZnO, are equal (4.073 Å) establishes that there is no zinc in the catalyst particles. As can be seen by constructing a Vegard's law relationship using Au-rich Au/Zn substitutional intermetallics with FCC superstructures [24], even 7% Zn in Au (approximately the maximum solid solubility at room temperature [20]) should result in a significant decrease in the lattice parameter of the Au nanoparticles to 4.0562 Å. Therefore, the Au catalyst particles have effectively no Zn.

If Zn is not alloying into the Au catalyst particles, it cannot be causing eutectic melting below the melting temperature of pure Au, as in the VLS synthesis mechanism. Decreasing particle size can also lower the melting temperature, but the effect is insufficient to cause melting at the synthesis temperature. According to the model of Buffat and Borel [25], 33 nm Au particles should melt at 1031 °C, well above the synthesis temperature of approximately 850 °C.

In order to verify the melting point of the Au catalyst particles, *in situ* XRD data were collected at elevated temperatures on the Au-catalysed ZnO nanorods. Offset 2θ scans of the Au{111} reflection were collected from 500 to 1000 °C, in 100° increments, seen in figure 4. The Au{111} reflection is present in all scans, including that at 1000 °C, indicating that the Au nanoparticles did not melt. Since the synthesis temperature was around 850 °C, it is likely that the Au catalyst particles remain solid during synthesis, indicating that growth is by the VSS synthesis mechanism, not the VLS synthesis mechanism.

The absence of Zn in the Au catalyst particle also indicates that growth cannot be proceeding by a supersaturation–nucleation process, as previously considered. A mass

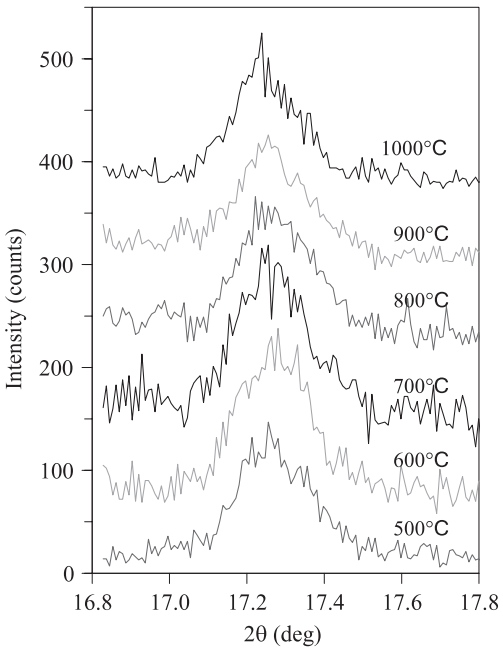

Figure 4. XRD patterns of the Au{111} reflection of Au-catalysed ZnO nanorods at temperatures of 500–1000 °C.

spectroscopy study of thermally evaporated ZnO [26] has shown that the ZnO dissociates into ionic species, which would be unlikely to diffuse into and alloy with metallic Au. It is more likely that growth proceeds by diffusion around the surface of the Au catalyst particle to the growing nanowire.

Wang and Fischman [27] and later Cheyssac *et al* [28] have proposed surface diffusion as a significant part of the VLS mechanism, supported by the fact that liquid surface diffusion rates are significantly higher than liquid bulk diffusion rates. The same holds true for solid surface and bulk diffusion; the surface diffusion coefficient of solid Au is several orders of magnitude greater than the bulk diffusion coefficient [29]. In addition, Au nanoparticles can have a disordered, quasi-liquid layer on the surface due to surface reconstruction [30, 31]. In other metals, such layers have been found to have unusually high self-diffusion coefficients at temperatures approaching the melting point [32].

4. Conclusions

Au-catalysed, vertically aligned ZnO nanowires were grown on an AlGaN/AlN layer on an (0001)-oriented Al_2O_3 single-crystal substrate. Using XRD texture analysis, the average orientation relationships over the entire sample were determined between the Al_2O_3, AlN, AlGaN, ZnO and Au phases, and were found to follow the lower lattice mismatch orientations. Most of the Au nanocrystals were observed to reconstruct from a polycrystalline orientation to a {111} orientation. The texture analysis also revealed two {111} orientations of the Au nanoparticles, related to each other by a 30° rotation about the sample normal.

The gold lattice parameter of the ZnO nanowire sample was determined to be the same as that of a control sample never exposed to vaporized ZnO, indicating the absence of any impurities, including Zn, in the Au catalyst particles. This suggests that the catalyst particle is solid during growth, since there will be no eutectic depression of the melting point, which is supported by high-temperature XRD results. Therefore, the growth is more properly described by the vapour–solid–solid (VSS) mechanism rather than the vapour–liquid–solid (VLS) mechanism in this case. The absence of Zn in the Au catalyst particle also suggests that growth proceeds by surface diffusion, rather than bulk diffusion.

References

[1] Wang Z L 2004 *J. Phys.: Condens. Matter* **16** R829–58
[2] Hsu C L, Chang S J, Lin Y R, Li P C, Lin T S, Tsai S Y, Lu T H and Chen I C 2005 *Chem. Phys. Lett.* **416** 75–8
[3] Kar S, Pal B N, Chaudhuri S and Chakravorty D 2006 *J. Phys. Chem.* B **110** 4605–11
[4] Wang Z L and Song J H 2006 *Science* **312** 242–6
[5] Gao P X, Song J, Liu J and Wang Z L 2006 *Adv. Mater.* **19** 67–72
[6] Rubio-Sierra F J, Heckl W M and Stark R W 2005 *Adv. Eng. Mater.* **7** 193–6
[7] He J H, Hsu J H, Wang C W, Lin H N, Chen L J and Wang Z L 2006 *J. Phys. Chem.* B **110** 50–3
[8] Morber J R, Ding Y, Haluska M S, Li Y, Liu J P, Wang Z L and Snyder R L 2006 *J. Phys. Chem.* B **110** 21672–9
[9] Cao L, Garipcan B, Atchison J S, Ni C, Nabet B and Spanier J E 2006 *Nano Lett.* **6** 1852–7
[10] Chang K W and Wu J J 2005 *J. Mater. Res.* **20** 3397–403
[11] Wagner R S and Ellis W C 1964 *Appl. Phys. Lett.* **4** 89–90
[12] Johansson J, Wacaser B A, Dick K A and Seifert W 2006 *Nanotechnology* **17** S355–61
[13] Persson A I, Larsson M W, Stenström S, Ohlsson B J, Samuelson L and Wallenberg L R 2004 *Nat. Mater.* **3** 677–81
[14] Dick K A, Deppert K, Karlsson L S, Larsson M W, Seifert W, Wallenberg L R and Samuelson L 2007 *Mater. Res. Bull.* **32** 127–33
[15] Dick K A, Deppert K, Karlsson L S, Wallenberg L R, Samuelson L and Seifert W 2005 *Adv. Funct. Mater.* **15** 1603–10
[16] Dick K A, Deppert K, Mårtensson T, Mandl B, Samuelson L and Seifert W 2005 *Nano Lett.* **5** 761–4
[17] Kamins T I, Williams R S, Basile D P, Hesjedal T and Harris J S 2001 *J. Appl. Phys.* **89** 1008–16
[18] Wang Y, Schmidt V, Senz S and Gösele U 2006 *Nat. Nanotechnol.* **1** 186–9
[19] Colli A, Hofmann S, Ferrari A C, Ducati C, Martelli F, Rubini S, Cabrini S and Franciosi A 2005 *Appl. Phys. Lett.* **86** 153103
[20] Liu H S, Ishida K, Jin Z P and Du Y 2003 *Intermetallics* **11** 987–94
[21] Wang X D, Song J H, Li P, Ryou J H, Dupuis R D, Summers C J and Wang Z L 2005 *J. Am. Chem. Soc.* **127** 7920–3
[22] Cullity B D and Stock S R 2001 *Elements of X-Ray Diffraction* (Englewood Cliffs, NJ: Prentice-Hall)
[23] Qi W H and Wang M P 2005 *J. Nanopart. Res.* **7** 51–7
[24] Iwasaki H 1962 *J. Phys. Soc. Japan* **17** 1620–33
[25] Buffat P and Borel J P 1976 *Phys. Rev.* A **13** 2287–98
[26] Makarow A V, Zbezhneva S G, Kovalenko V V and Rumyantseva M N 2003 *Inorg. Mater.* **39** 594–8
[27] Wang H and Fischman G S 1994 *J. Appl. Phys.* **76** 1557–62
[28] Cheyssac P, Sacilotti M and Patriarche G 2006 *J. Appl. Phys.* **100** 044315
[29] Beszeda I, Szabó I A and Gontier-Moya E G 2004 *Appl. Phys.* A **78** 1079–84
[30] Ajayan P M and Marks T J 1989 *Phys. Rev. Lett.* **63** 279–82
[31] Krakow W, Jóse-Yacamán M and Aragón J L 1994 *Phys. Rev.* B **49** 591–6
[32] Frenken J W M, Toennies J P and Wöll C 1988 *Phys. Rev. Lett.* **60** 1727–30